ACS Photonics

Article

pubs.acs.org/journal/apchd5

Dynamics of Large Femtosecond Filament Arrays: Possibilities, Limitations, and Trade-Offs

Wiktor Walasik and Natalia M. Litchinitser*

Department of Electrical Engineering, University at Buffalo, The State University of New York, Buffalo, New York 14260, United States

ABSTRACT: Stable propagation of large, multifilament arrays over long distances in air paves new ways for microwave-radiation manipulation. Although the dynamics of a single or a few filaments has been discussed in previous studies, we show that the stability of large plasma-filament arrays is significantly more complicated and is constrained by several trade-offs. Here, we analyze the stability properties of rectangular arrays as a function of four parameters: relative phase of the generating beams, number of filaments, separation between them, and initial power. We find that arrays with an alternating filament phase are more stable than similar arrays with all beams in phase. Additionally, we show that increasing the size of an array increases its stability and that a proper choice of the beam separation and the initial power has to be made in order to obtain a dense and regular array of filaments.

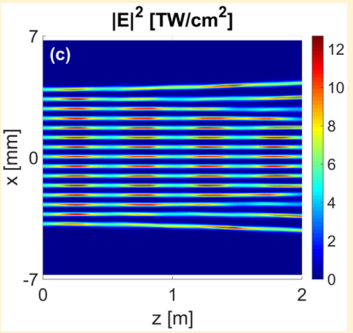

KEYWORDS: *filamentation in plasmas, dynamics of nonlinear optical systems, optical instabilities, optical chaos, optical spatiotemporal dynamics, optical solitons, nonlinear guided waves, beam trapping, self-focusing, self-phase modulation*

High-power femtosecond laser-pulse filamentation is a flourishing field of nonlinear optics due to its numerous applications in remote sensing, lightning protection, virtual antennas, and waveguiding.[1−3] Experiments show that femtosecond laser beams can ionize atmosphere at kilometer-scale distances.[4] Propagation over such long distances is a result of the dynamic balance between the focusing Kerr nonlinearity, diffraction, and plasma defocusing due to multiphoton absorption. A proper arrangement of plasma channels into arrays built of multiple filaments can lead to control[5] and efficient guiding of electromagnetic radiation in air.[6] Dielectric[7] and hollow-core metallic waveguide configurations[8,9] were predicted theoretically and demonstrated experimentally[10] to guide microwave radiation. Periodic arrays of densely packed high-intensity filaments were shown to create a hyperbolic metamaterial medium, which allows for radar-signal manipulation and resolution enhancement.[11,12]

Formation of desired, regular filament patterns requires precise control of filament distribution and interaction. Multiple filaments can be generated by an intense Gaussian beam,[13,14] whose power is much higher than the critical power of self-focusing P_{cr}. However, the distribution of filaments resulting from the breakup of a Gaussian beam is determined by intensity fluctuations[15] and modulation instability.[16,17] Moreover, the density of filaments generated in this way is limited.[18,19] Therefore, this method can not provide the fine control and the high filament density required for the microwave-radiation manipulation. A certain degree of control of the filament distribution can be obtained by special preparation of the Gaussian beam. It was demonstrated experimentally that the predetermined initial phase,[20,21] amplitude distribution,[15] and geometry of the beam[22] offer a limited control of the filamentation pattern. The filament distribution in an array can be even more deterministic if the position of each beam is managed independently. This is obtained by multiple beam generation using arrays of axicons[23,24] or microlenses.[25−28]

The question motivating our study is how to ensure that the initial multifilament distribution remains unchanged during the propagation or evolves in a predictable manner. This evolution is governed by the stability of a single filament in the array and by the mutual interaction between the neighboring filaments. The majority of studies of filament interaction have focused only on two-beam interaction, which has been shown to result in attraction or repulsion of the filaments depending on their phase difference,[29,30] or rotation of the filament pattern.[31,32] Studies of two beams give a basic understanding of the filament interaction, but do not provide the insight on the interaction of beams in two-dimensional (2D) arrays built of multiple filaments.

In this paper, we present a comprehensive study of the stability of large 2D arrays of filaments. We analyze the effects of the relative phase difference between the beams in the array on the propagation dynamics. Moreover, we study the effects related with the size of the array, the density of beams (separation distance), and the initial power. In particular, we show that arrays built of out-of-phase filaments are more robust than these with all filaments in phase. Additionally, an increase in array size and a careful choice of the power and the beam separation allow us to increase the propagation distance over which the array of the beams propagates in a stable and predictable manner. This study provides guidance in selecting parameters for future experiments with large filament arrays.

Received: December 18, 2015
Published: March 2, 2016

DOI: 10.1021/acsphotonics.5b00734
ACS Photonics 2016, 3, 640−646

This paper is organized in the following way. First, we briefly discuss the general properties of structures that can be created using large arrays of plasma filaments in air, motivating our study on how to enable generation of stable arrays with requisite properties. Next, we describe methods used in our simulations and parameters of the studied system. Then, we investigate the difference in propagation dynamics of filament arrays with all the beams in phase and the arrays with alternating phase of the neighboring beams (out-of-phase arrays). Later, we analyze the stability of arrays with different number of beams, beam separation, and initial power for the out-of-phase arrays.

METHODS

Arrays of filaments, like the one presented in Figure 1a, are able to create strongly anisotropic media, such as an elliptical or hyperbolic medium. In the effective medium approximation, the diagonal elements of the permittivity tensor of such arrays are given by

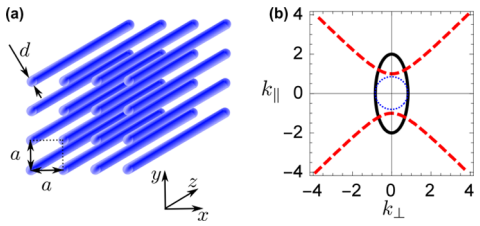

Figure 1. (a) Schematic illustration of the metamaterial formed by laser-induced plasma filaments (blue wires). The diameter of a filament is denoted as d, and a represents separation between filaments. (b) Typical isofrequency contours for isotropic ($\epsilon_\perp = \epsilon_\|$; blue dotted curve), elliptical ($0 < \epsilon_\| < \epsilon_\perp$; black solid curve), and hyperbolic ($\epsilon_\| < 0 < \epsilon_\perp$; red dashed curve) medium.

$$\epsilon_{xx} = \epsilon_{yy} = \epsilon_\perp = \epsilon_h \frac{(1+f)\epsilon_{\text{fil}} + (1-f)\epsilon_h}{(1-f)\epsilon_{\text{fil}} + (1+f)\epsilon_h} \tag{1a}$$

$$\epsilon_{zz} = \epsilon_\| = f\epsilon_{\text{fil}} + (1-f)\epsilon_h \tag{1b}$$

where $f = \pi[d/(2a)]^2$ denotes the filament filing fraction, a represents the separation between the filaments in a square lattice, and d is the filament diameter. Here, ϵ_h is the host medium permittivity and ϵ_{fil} is the permittivity of a filament. Filament permittivity can be described by the Drude model, in which the plasma frequency is related to the electron density in the plasma generated in a filament. The dispersion of extraordinary waves propagating in the z-direction in such a uniaxial medium is characterized by

$$\frac{k_\|^2}{\epsilon_\perp} + \frac{k_\perp^2}{\epsilon_\|} = \frac{\omega^2}{c^2} \tag{2}$$

Typical solutions of eq 2 are shown in Figure 1b.

In order to study the nonlinear dynamics of filament propagation, we use the $(3+1)D$ nonlinear Schrödinger equation with the typical parameters for air:[2,33]

$$\frac{\partial E}{\partial z} = \frac{i}{2k_0}\left(\frac{\partial^2}{\partial x^2} + \frac{\partial^2}{\partial y^2}\right)E - i\frac{k''}{2}\frac{\partial^2 E}{\partial t^2} + ik_0 n_2 \mathcal{R}(t)E - \left(\frac{\sigma_B}{2} + i\frac{k_0}{2\rho_c}\right)\rho E - \frac{\beta^{(K)}}{2}|E|^{2K-2}E \tag{3}$$

where the slowly varying electric-field envelope E is normalized in such a way that $|E|^2$ is the light intensity expressed in W/m^2. $k_0 = 2\pi/\lambda$ denotes the free-space wavevector, and $\lambda = 775$ nm is the free-space wavelength. The group velocity dispersion is given by $k'' = 0.2$ fs^2/cm, and the Kerr nonlinear parameter is $n_2 = 5.57 \times 10^{-19}$ cm^2/W. The inverse Bremsstrahlung cross-section responsible for plasma absorption is denoted by $\sigma_B = 5.54 \times 10^{-20}$ cm^2, and the critical plasma density at which air becomes transparent is given by $\rho_c = 1.86 \times 10^{-21}$ cm^{-3}. The multiphoton absorption coefficient is given by $\beta^{(K)} = 3.1 \times 10^{-95}$ cm^{13}/W^7, where $K = 8$ is the number of photons needed to overcome the ionization potential $U_i = 12$ eV. The time evolution of the electron density ρ is governed by equation

$$\frac{\partial \rho}{\partial t} = \sigma_K \rho_{\text{nt}} |E|^{2K} + \frac{\sigma_B}{U_i}\rho|E|^2 \tag{4}$$

where $\sigma_K = \beta^{(K)}/(K\hbar\omega\rho_{\text{nt}})$ is the multiphoton ionization coefficient, $\hbar\omega$ denotes the energy of a single photon at the wavelength $\lambda = 2\pi c/\omega$, and $\rho_{\text{nt}} = 5.4 \times 10^{18}$ cm^{-3} is the density of neutral oxygen molecules. Function

$$\mathcal{R}(t) = (1-\alpha)|E(t)|^2 + \frac{\alpha}{\tau_K}\int_{-\infty}^{t} e^{-(t-\tau)/\tau_K}|E(\tau)|^2 d\tau \tag{5}$$

models Kerr and noninstantaneous nonlinear responses.[33] Here, $\alpha = 0.5$ is the fraction of the delayed nonlinear response due to stimulated molecular Raman scattering, and $\tau_K = 70$ fs denotes the characteristic relaxation time for oxygen molecules. For these parameters, the clamping intensity is $I_c = 31$ TW/cm^2.

Solving numerically the full $(3+1)D$ nonlinear Schrödinger equation is a very time and memory consuming process.[33] Therefore, we will simplify the problem using a reduced model proposed in ref 33. This model has been successfully used in studies of multiple filamentation, for instance, in refs 24, 30, 31, and 34. Here, we recapitulate the derivation of the reduced model along the lines presented in ref 33.

We assume that the temporal distribution of the filament electric field can be described by a dominant Gaussian spike centered at a time instant $t_c(z)$ with a time extent T:

$$E(x, y, z, t) = \psi(x, y, z)\exp\left[-\frac{[t - t_c(z)]^2}{T^2}\right] \tag{6}$$

Here, $\psi(x,y,z)$ describes the spatial distribution of the electric field and $T = 0.1t_p$, where $t_p = 85$ fs is the duration of the pulse exciting the filament. The compression factor 0.1 was shown in ref 33 to provide the best approximation of the full $(3+1)D$ model. Under this assumption, eq 4 can be readily integrated to give

$$\rho = \frac{\sqrt{\pi}\, T\sigma_K \rho_{\text{nt}} |\psi|^{2K}}{\sqrt{8K}}\left(\text{erf}\left\{\frac{\sqrt{2K}\,[t - t_c(z)]}{T}\right\} + 1\right) \tag{7}$$

Equation 7 suggests that, for all the time instances larger than $t_c + 3T$, the electron density ρ remains at the maximum level as the electron recombination processes are not taken into account. Full description of electron density should include the decay rate equations. However, the characteristic electron density decay time was predicted and confirmed experimentally to be of the order of 100 ps,[35,36] which is at least 3 orders of magnitude larger than the time scales for filament formation considered here.

In the following derivation, we neglect the dispersion term whose effects on the filament evolution are much smaller than these connected with ionization.[33] The plasma absorption is also

DOI: 10.1021/acsphotonics.5b00734
ACS Photonics 2016, 3, 640−646

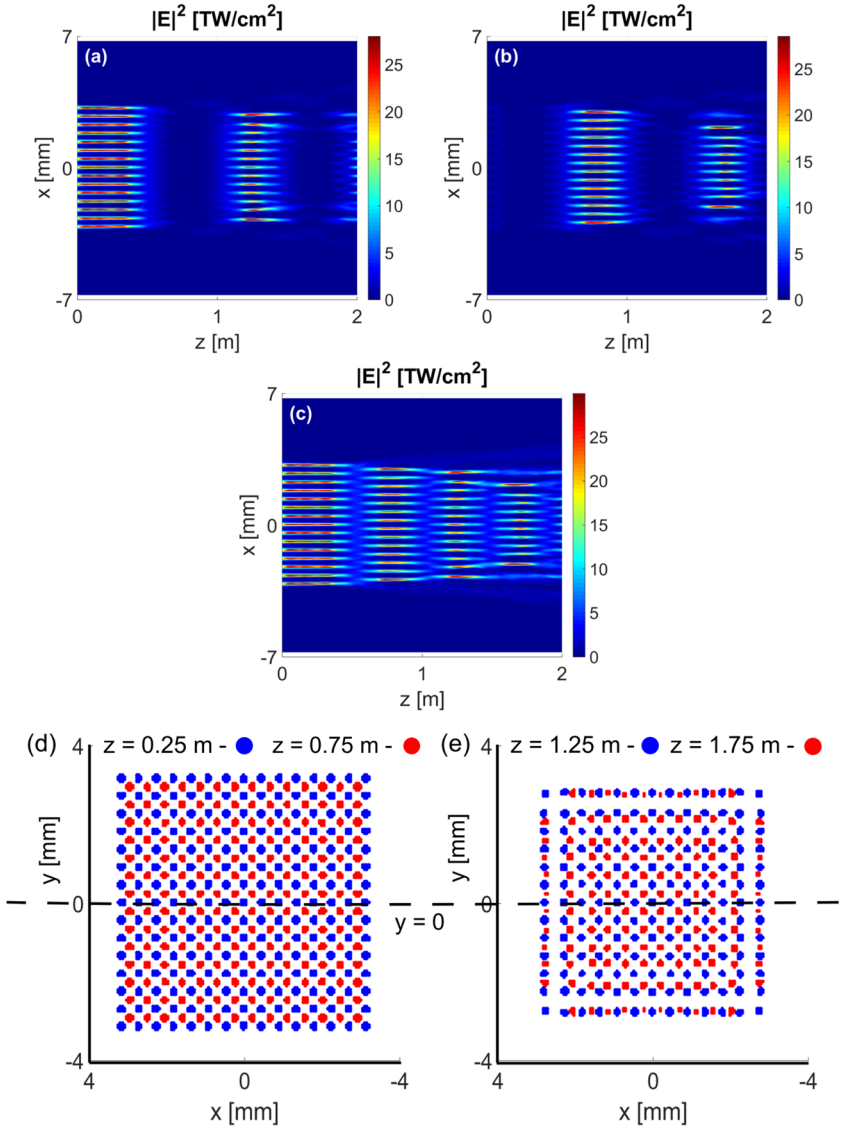

Figure 2. (a–c) Filament intensity distributions: (a) $|E(x,y = 0,z)|^2$, (b) $|E(x,y = a/2,z)|^2$, (c) average of intensities presented in panels (a) and (b) for the in-phase 15 × 15 beam array. (d–e) Superimposed filament location in the transverse plane at four different propagation distances: (d) $z = 0.25$ m (blue) and $z = 0.75$ m (red); (e) $z = 1.25$ m (blue) and $z = 1.75$ m (red). We assume that the filament is formed when the light intensity is higher than $I_c/8$. Arrays parameters are the following: the normalized initial power per beam $P_{in} = 4$, the width of a single beam $\sigma = 0.15$ mm, and the separation between beams $a = 0.45$ mm.

neglected, as it remains small compared to the multiphoton absorption. Inserting eqs 6 and 7 into eq 3 multiplied by $e^{-[t-t_c(z)]^2/T^2}$ and integrating over the entire time domain yields the equation for ψ:

$$\frac{\partial \psi}{\partial z} = \frac{i}{2k_0}\left(\frac{\partial^2}{\partial x^2} + \frac{\partial^2}{\partial y^2}\right)\psi + i\theta k_0 n_2 |\psi|^2\psi - i\gamma|\psi|^{2K}\psi - \frac{\beta^{(K)}}{2\sqrt{K}}|\psi|^{2K-2}\psi \tag{8}$$

where the time-averaged nonlinear response is quantified by $\theta = [1 - \alpha + \alpha D/(\sqrt{2}\,\tau_K)]/\sqrt{2}$, the time-averaged loss coefficient is $\gamma = (\sqrt{\pi/(8K)}\,Tk_0\sigma_K\rho_{nt})/(2\rho_c)$, and

$$D = \int_{-\infty}^{+\infty} \exp\left[\frac{T^2}{8\tau_K^2} - \frac{u}{\tau_K} - 2\left(\frac{u}{T}\right)^2\right] \times \left[\operatorname{erf}\left(\frac{\sqrt{2}\,u}{T} - \frac{T}{\sqrt{8}\,\tau_K}\right) + 1\right] du \tag{9}$$

The reduced model results in a 3D time-averaged nonlinear Schrödinger equation (eq 8). In order to study the evolution of the multifilament arrays, we solve eq 8 using split-step Fourier method.[37,38]

The input field distribution $\psi(x,y,0)$ is described as a sum of Gaussian beams organized in a rectangular lattice:

$$\psi(x, y, 0) = A\sum_{i=1}^{N_b} p^i \exp\left[-\frac{(x - x_{0,i})^2 + (y - y_{0,i})^2}{\sigma^2}\right] \tag{10}$$

where N_b denotes the number of beams and p^i is the phase of the ith beam. In an in-phase array, all of the beams have the same phase and $p = 1$. On the contrary, in an out-of-phase array, each beam has the phase opposite to its nearest neighbors; therefore (for rectangular arrays with odd numbers of beams studied here), $p = -1$. σ is the $1/e$ beam width and a pair $[x_{0,i}, y_{0,i}]$ denotes the location of the center of the ith beam in the transverse plane. The

DOI: 10.1021/acsphotonics.5b00734
ACS Photonics 2016, 3, 640–646

field amplitude A is related to the initial power. The initial power per beam normalized to the critical power in air $P_{cr} = 3.77\lambda^2/(8\pi n_2) = 1.6$ GW is calculated as

$$P_{in} = \frac{1}{P_{cr}N_b}\int_{-\infty}^{\infty}\int_{-\infty}^{\infty}\psi(x, y, 0)\mathrm{d}x\mathrm{d}y \quad (11)$$

In our studies, input beams have a spatial width of $\sigma = 0.15-0.20$ mm, which is approximately twice the width of a filament. Intensity distributions similar to our inputs were generated by a wide Gaussian beam impinging on an array of microlenses.[25,26,28]

RESULTS AND DISCUSSION

Let us first consider a large (15×15) in-phase array of Gaussian beams forming filaments. Figure 2a shows the light intensity distribution $|E(x,z)|^2$ in the plane $y = 0$, which crosses the centers of the middle column of beams exciting the filament array. Figure 2b shows $|E(x,z)|^2$ in the plane $y = a/2$ (a denotes the spacing between the filaments), which lays in between the two middle columns of exciting beams. Figure 2c shows the intensity distribution averaged over the two planes $y = 0$ and $y = a/2$. Figure 2d,e shows the location of the beams in the transverse plane $(x-y)$ for different values of the propagation distance z. All these figures considered together reveal the full dynamics of an in-phase filament array. At the beginning of the propagation ($z = 0-0.5$ m), a regular 15×15 array of filaments is formed, and the central beams lay in the plane $y = 0$. Because all the beams in the array have the same phase, their mutual interaction results in attraction of the neighboring beams, which fuse at $z \approx 0.5$ m. This results in a smaller array of 14×14 beams shown in Figure 2d in red. None of the beams in this array are located in $y = 0$ plane. This is the reason for the apparent light intensity decrease in the map shown in Figure 2a as the filaments are located in planes shifted by $a/2$ and are visible in Figure 2b. Similar fusion process leads to the generation of a 13×13 array (shown in blue in Figure 2e) visible in Figure 2a and a 12×12 array (shown in red in Figure 2e) visible in Figure 2b. As a result of mutual filament attraction, the array of the in-phase beams decreases in size and loses its regularity. The outer beams increase their distance from the center of the array, dissipate the energy, and are unable to reform filaments, which accelerates shrinking process of the array.

In order to compare the in-phase and the out-of-phase arrays, we study an array with the same parameters as those used in Figure 2 but with the alternate phase of the beams. Such a phase distribution is schematically presented in Figure 3a. The nearest neighbors of each of the beams are out-of-phase with the center beam, forming a chessboard-like pattern. Figure 3b shows the light intensity distribution $|E(x,z)|^2$ in the plane $y = 0$ for the out-of-phase array of beams. This time, beams do not merge and the number of filaments in the array is conserved during the propagation. This is the result of the mutual repulsion between the nearest-neighbor out-of-phase beams. The peak intensity of light in the filament beams oscillates during the propagation and reflects the dynamic balance between the Kerr focusing and the plasma defocusing. Due to their mutual repulsion, the outer beams increase their distance from the center of the array even faster than in the case of the in-phase array. Nevertheless, the out-of-phase array offers a significantly more stable behavior than the in-phase array since the number of filaments and the position of beams far from the edges of the array do not change. The stability of the two types of arrays can be also compared using the averaged filing fraction of filaments $\langle f \rangle$ shown in Figure 3c. The

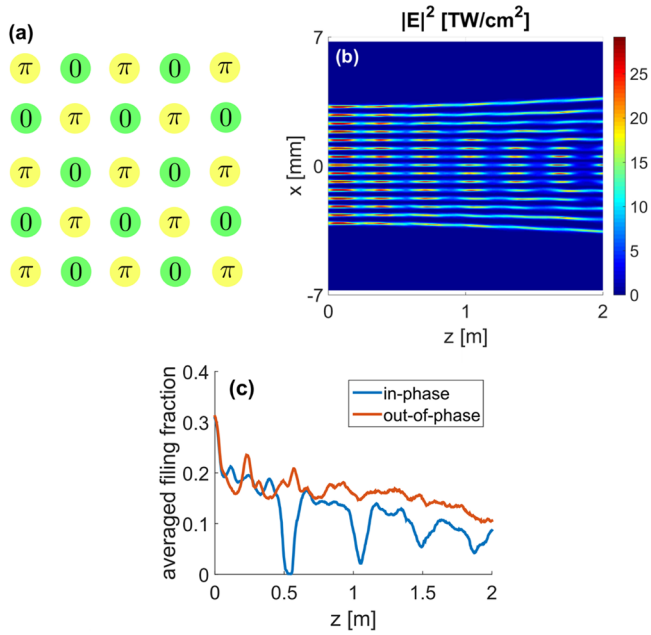

Figure 3. (a) Chessboard-like phase distribution in the out-of-phase filament array. (b) Filament intensity distribution $|E(x,y = 0,z)|^2$ for the out-of-phase 15×15 beam array. Other parameters of the array are identical to these in Figure 2. (c) Comparison of the averaged filament filing fraction $\langle f \rangle$ as a function of propagation distance z for the out-of-phase 15×15 array and the in-phase array presented in Figure 2.

averaged filing fraction is computed as a ratio between the transverse area where the filaments are present and the area of the whole array (the area of the array may increase during the propagation due to the divergence of beams located close to the edges of the array). The presence of a filament is determined by the fact that the light intensity at a given position is higher than a certain threshold value. In this study, we chose this threshold to be 1/8 of the clamping intensity I_c. For the in-phase array, the filing fraction decreases and experiences abrupt changes when array modifies its structure (when filaments merge). The decrease of the filing fraction of the out-of-phase array is much more uniform. In the later stages of propagation ($z = 1-2$ m), the filing fraction for the out-of-phase array is on average 1.5× higher than for the in-phase array. These results suggest that the out-of-phase arrays are generally more stable than the in-phase arrays; therefore, further discussion will focus on the out-of-phase arrays.

Let us analyze the stability of the out-of-phase filament array as a function of the number of beams building it. Figure 4 shows the dynamics of arrays with different sizes. We show that the larger the array, the more stable it is. Small arrays, built of 9 or 25 beams, tend to destabilize faster than larger arrays. We notice that the outer filaments increase their distance from the center of the array and then lose the energy due to diffraction. This effect can be explained in the following way. The most stable filaments are those in the middle of an array since they have all four (out-of-phase) nearest neighbors. Each of these neighbors repulses the central filament, but the net force is zero due to symmetry reasons. The filaments on the edges and corners are more susceptible to transverse displacement as they only have three or two nearest neighbors, and the net repulsive force acting on them is nonzero. The larger the array, the higher the ratio between the bulk and edge filaments is and, consequently, the better the stability of the filament array. The fact that the stability of the arrays increases with their size is a very desirable property from

DOI: 10.1021/acsphotonics.5b00734
ACS Photonics 2016, 3, 640−646

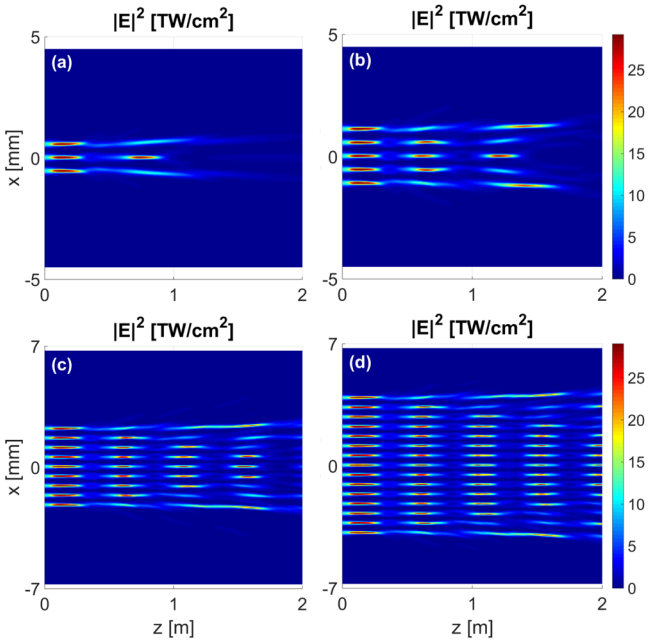

Figure 4. Light intensity distribution in the $y = 0$ plane for filament arrays of different sizes (number of beams N_b): (a) $3 \times 3 = 9$, (b) $5 \times 5 = 25$, (c) $9 \times 9 = 81$, and (d) $15 \times 15 = 225$. In each array $P_{in} = 4$, the beam separation is $a = 0.55$ mm, and the width of a single beam $\sigma = 0.2$ mm. The x range is different for plots (a), (b) and (c), (d).

an experimental point of view, as the manipulation of microwave beams requires large beam arrays that are uniform or evolve in a predictable manner.

Next, we will study the behavior of the beam array as a function of the separation between the neighboring filaments. The separation of the beams determines the filing fraction of filaments, which is a critical parameter for the properties of filament-based waveguides and metamaterials.[11] From a practical viewpoint, high filing fractions are necessary for efficient microwave beam guiding and manipulation. However, as Figure 5 shows, the increase of the filing fraction decreases the stability of the filament array. As a consequence of a decreased beam separation, the filament-filament interaction becomes stronger, and the array broadens. This effectively decreases the filing fraction as it can be seen from Figure 5e. The arrays with the smallest beam separations have the highest filing fraction in the first 1 m of propagation. However, due to the rapid broadening of these arrays, the filing fraction decreases, and at $z = 2$ m, it is equal to the values obtained for arrays with larger beam separation. Therefore, the trade-off between the need for a high filing fraction and the array-size evolution should be taken into account. The oscillations of the peak intensity of filaments are also reflected in the filing fraction. They are especially visible for arrays with larger beam separation, for which the filing fraction oscillates during the propagation. This result shows that, for arrays with $P_{in} = 4$, the filling fraction of densely packed filaments behaves more monotonically than for sparse arrays but experiences a larger overall decrease during the entire propagation distance studied here.

Finally, we study the behavior of the filament array as a function of the initial power used to generate the array. As shown in Figure 6, at low powers ($P_{in} = 0.5$ or 1), the outer beams diverge away from the array center in early stages of propagation and diffract rapidly as the power is too low to create a filament. For a chosen beam width $\sigma = 0.2$ mm, the most stable

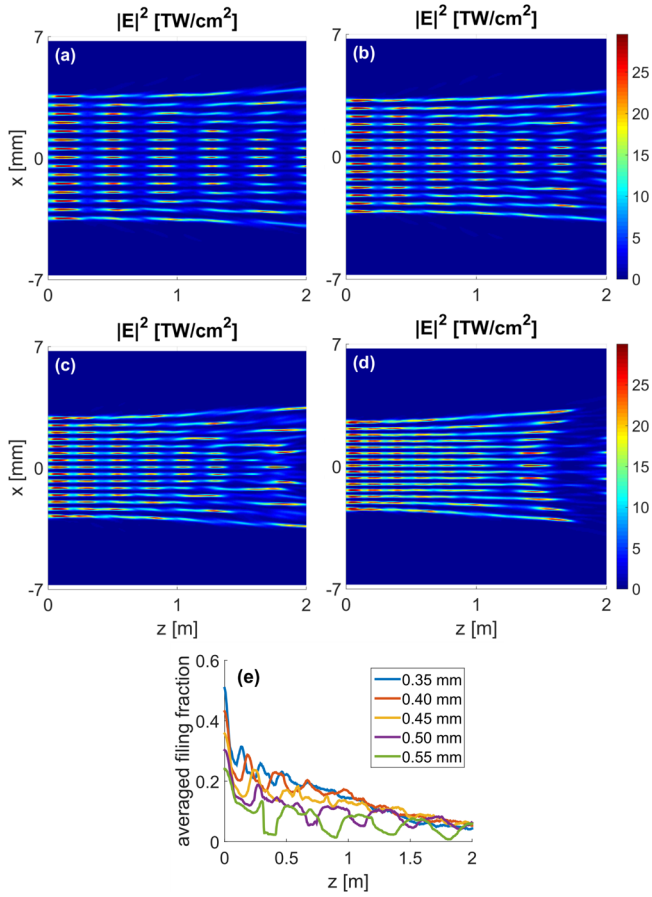

Figure 5. Light intensity distribution in the $y = 0$ plane for large (15×15) filament arrays with different beam separation a: (a) 0.50, (b) 0.45, (c) 0.40, and (d) 0.35 mm. The evolution of an array with $a = 0.55$ mm is presented in Figure 4d. In each array, $P_{in} = 4$ and the width of a single beam is $\sigma = 0.2$ mm. (e) Comparison of the averaged filament filing fraction $\langle f \rangle$ as a function of propagation distance z for the out-of-phase 15×15 arrays with different initial beam separation.

propagation of a single beam is obtained for $P_{in} = 1$ (see Figure 6b). It results in a practically constant peak intensity of beams close to the array center. However, the peak intensity obtained at $P_{in} = 1$ is 10× lower than the saturation intensity of a filament reached for arrays excited with high powers ($P_{in} = 4$ or 8). In high-power regime, the divergence and diffraction of the outer filaments is slower than for low-power arrays, but the oscillations of the peak intensity have higher amplitudes. These results suggest another trade-off between the uniformity of a single filament and the array as a whole. A power level resulting in a proper balance between the regularity of the whole array and the uniformity of a single filament should be chosen in experimental studies.

In conclusion, inspired by the possibility of designing large arrays of filaments for microwave manipulation, we have systematically studied the propagation of large arrays of femtosecond laser beams in air. We have analyzed the effect of the relative phase difference between the filaments in the array and found out that the arrays with a chessboard-like out-of-phase beam arrangement propagate unchanged for longer distances than the in-phase arrays. The in-phase arrays tend to reduce their size during the propagation due to mutual attraction and resulting fusion of the filaments. Furthermore, for the out-of-phase arrays, we have analyzed the dependence of their stability

DOI: 10.1021/acsphotonics.5b00734
ACS Photonics 2016, 3, 640−646

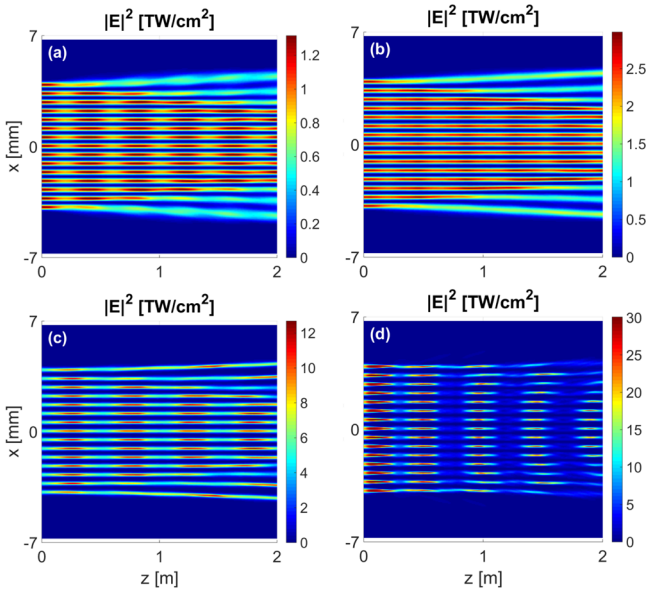

Figure 6. Light intensity distribution in the $y = 0$ plane for large (15×15) filament arrays with different values of initial power P_{in}: (a) 0.5, (b) 1, (c) 2, and (d) 8. In each array the separation between beams is equal to $a = 0.55$ mm and the width of a single beam $\sigma = 0.2$ mm. The evolution of an array with initial power of $P_{in} = 4$ is presented in Figure 4d.

on the following parameters: the number of beams building an array, the separation between the beams, and the initial power per beam. Our studies have shown that the increase of the number of filaments leads to longer stable propagation of an array. Similar stability enhancement of the array as a whole was observed with the increase of the excitation power; however, the oscillations of intensity inside a single filament increased at the same time. Moreover, we have shown that the reduction of the separation between the filaments has two effects: on the one hand it increases the filament filing fraction and reduces its oscillations during the propagation; on the other hand, it accelerates the increase of the array transverse size. All of the effects discussed above influence the attainable filament filing fraction and have a crucial importance for experimental realization of filament-based metamaterials.

AUTHOR INFORMATION

Corresponding Author

*E-mail: natashal@buffalo.edu.

Notes

The authors declare no competing financial interest.

ACKNOWLEDGMENTS

This work was supported by U.S. Army Research Office Grants #W911NF-15-1-0146 and MURI #W911NF-11-0297.

REFERENCES

(1) Fibich, G.; Ilan, B. Vectorial and random effects in self-focusing and in multiple filamentation. *Phys. D* **2001**, *157*, 112.

(2) Couairon, A.; Mysyrowicz, A. Femtosecond filamentation in transparent media. *Phys. Rep.* **2007**, *441*, 47.

(3) Chin, S.; Wang, T.-J.; Marceau, C.; Wu, J.; Liu, J.; Kosareva, O.; Panov, N.; Chen, Y.; Daigle, J.-F.; Yuan, S.; Azarm, A.; Liu, W.; Seideman, T.; Zeng, H.; Richardson, M.; Li, R.; Xu, Z. Advances in intense femtosecond laser filamentation in air. *Laser Phys.* **2012**, *22*, 1.

(4) Durand, M.; Houard, A.; Prade, B.; Mysyrowicz, A.; Durécu, A.; Moreau, B.; Fleury, D.; Vasseur, O.; Borchert, H.; Diener, K.; Schmitt, R.; Théberge, F.; Chateauneuf, M.; Daigle, J.-F.; Dubois, J. Kilometer range filamentation. *Opt. Express* **2013**, *21*, 26836−26845.

(5) Marian, A.; Morsli, M. E.; Vidal, F.; Payeur, S.; Châteaumeuf, M.; Théberge, F.; Dubois, J.; Kieffer, J.-C. The interaction of polarized microwaves with planar arrays of femtosecond laser-produced plasma filaments in air. *Phys. Plasmas* **2013**, *20*, 023301.

(6) Jhajj, N.; Rosenthal, E. W.; Birnbaum, R.; Wahlstrand, J. K.; Milchberg, H. M. Demonstration of long-lived high-power optical waveguides in air. *Phys. Rev. X* **2014**, *4*, 011027.

(7) Alshershby, M.; Lin, J.; Hao, Z. Numerical analysis of guiding a microwave radiation using a set of plasma filaments: dielectric waveguide concept. *J. Phys. D: Appl. Phys.* **2012**, *45*, 065102.

(8) Musin, R. R.; Shneider, M. N.; Zheltikov, A. M.; Miles, R. B. Guiding radar signals by arrays of laser-induced filaments: finite-difference analysis. *Appl. Opt.* **2007**, *46*, 5593.

(9) Alshershby, M.; Hao, Z.; Lin, J. Guiding microwave radiation using laser-induced filaments: the hollow conducting waveguide concept. *J. Phys. D: Appl. Phys.* **2012**, *45*, 265401.

(10) Châteauneuf, M.; Payeur, S.; Dubois, J.; Kieffer, J.-C. Microwave guiding in air by a cylindrical filament array waveguide. *Appl. Phys. Lett.* **2008**, *92*, 091104.

(11) Kudyshev, Z. A.; Richardson, M. C.; Litchinitser, N. M. Virtual hyperbolic metamaterials for manipulating radar signals in air. *Nat. Commun.* **2013**, *4*, 2557.

(12) Will, S.; Kudyshev, Z. A.; Litchinitser, N. M. Free-space components for microwave transmission. *Phot. Nano. Fundam. Appl.* **2015**, *13*, 1.

(13) Bergé, L.; Skupin, S.; Lederer, F.; Méjean, G.; Yu, J.; Kasparian, J.; Salmon, E.; Wolf, J. P. Spatial Break-up of Femtosecond Laser Pulses in the Atmosphere. *Phys. Scr.* **2004**, *T107*, 135.

(14) Fibich, G.; Eisenmann, S.; Ilan, B.; Zigler, A. Control of multiple filamentation in air. *Opt. Lett.* **2004**, *29*, 1772.

(15) Méchain, G.; Couairon, A.; Franco, M.; Prade, B.; Mysyrowicz, A. Organizing Multiple Femtosecond Filaments in Air. *Phys. Rev. Lett.* **2004**, *93*, 035003.

(16) Bespalov, V. I.; Talanov, V. I. Filamentary structure of light beams in nonlinear liquids. *Zh. Eksper. Teor. Fiz. Pis'ma* **1966**, *3*, 471.

(17) Zakharov, V.; Ostrovsky, L. Modulation instability: The beginning. *Phys. D* **2009**, *238*, 540.

(18) Henin, S.; Petit, Y.; Kasparian, J.; Wolf, J.-P.; Jochmann, A.; Kraft, S. D.; Bock, S.; Schramm, U.; Sauerbrey, R.; Nakaema, W. M.; Stelmaszczyk, K.; Rohwetter, P.; Wöste, L.; Soulez, C.-L.; Mauger, S.; Bergé, L.; Skupin, S. Saturation of the filament density of ultrashort intense laser pulses in air. *Appl. Phys. B: Lasers Opt.* **2010**, *100*, 77.

(19) Ettoumi, W.; Kasparian, J.; Wolf, J.-P. Laser Filamentation as a New Phase Transition Universality Class. *Phys. Rev. Lett.* **2015**, *114*, 063903.

(20) Liu, L.; Wang, C.; Cheng, Y.; Gao, H.; Liu, W. Fine control of multiple femtosecond filamentation using a combination of phase plates. *J. Phys. B: At., Mol. Opt. Phys.* **2011**, *44*, 215404.

(21) Gao, H.; Chu, W.; Yu, G.; Zeng, B.; Zhao, J.; Wang, Z.; Liu, W.; Cheng, Y.; Xu, Z. Femotosecond laser filamentat array generated with step phase plate in air. *Opt. Express* **2013**, *21*, 4612.

(22) Dubietis, A.; Tamosauskas, G.; Fibich, G.; Ilan, B. Multiple filamentation induced by input-beam ellipticity. *Opt. Lett.* **2004**, *29*, 1126.

(23) Sun, X.; Gao, H.; Zeng, B.; Xu, S.; Liu, W.; Cheng, Y.; Xu, Z.; Mu, G. Multiple filamentation generated by focusing femtosecond laser with axicon. *Opt. Lett.* **2012**, *37*, 857.

(24) Sun, X.; Gao, H.; Zhang, S.; Liu, W. Numerical simulation of the generation of multiple laser filaments by an axicon array. *J. Mod. Opt.* **2013**, *60*, 1637.

(25) Camino, A.; Hao, Z.; Liu, X.; Lin, J. Control of laser filamentation in fused silica by a periodic microlens array. *Opt. Express* **2013**, *21*, 7908.

(26) Camino, A.; Hao, Z.; Liu, X.; Lin, J. High spectral power femtosecond supercontinuum source by use of microlens array. *Opt. Lett.* **2014**, *39*, 747.

DOI: 10.1021/acsphotonics.5b00734
ACS Photonics 2016, 3, 640−646

(27) Camino, A.; Xi, T.; Hao, Z.; Lin, J. Femtosecond filament array generated in air. *Appl. Phys. B: Lasers Opt.* **2015**, *121*, 363.
(28) Xi, T.; Zhao, Z.; Hao, Z. Femtosecond laser filamentation with a microlens array in air. *J. Opt. Soc. Am. B* **2015**, *32*, 163.
(29) Cai, H.; Wu, J.; Lu, P.; Bai, X.; Ding, L.; Zeng, H. Attraction and repulsion of parallel femtosecond filaments in air. *Phys. Rev. A: At., Mol., Opt. Phys.* **2009**, *80*, 051802(R).
(30) Ma, Y.-Y.; Lu, X.; Xi, T.-T.; Gong, Q.-H.; Zhang, J. Filamentation of interacting femtosecond laser pulses in air. *Appl. Phys. B: Lasers Opt.* **2008**, *93*, 463.
(31) Shim, B.; Schrauth, S. E.; Hensley, C. J.; Vuong, L. T.; Hui, P.; Ishaaya, A. A.; Gaeta, A. L. Controlled interactions of femtosecond light filaments in air. *Phys. Rev. A: At., Mol., Opt. Phys.* **2010**, *81*, 061803(R).
(32) Barbieri, N.; Hosseinimakarem, Z.; Lim, K.; Durand, M.; Baudelet, M.; Johnson, E.; Richardson, M. Helical filaments. *Appl. Phys. Lett.* **2014**, *104*, 261109.
(33) Skupin, S.; Bergé, L.; Peschel, U.; Lederer, F.; Méjean, G.; Yu, J.; Kasparian, J.; Salmon, E.; Wolf, J. P.; Rodriguez, M.; Wöste, L.; Bourayou, R.; Sauerbrey, R. Filamentation of femtosecond light pulses in the air: Turbulent cells versus long-range clusters. *Phys. Rev. E* **2004**, *70*, 046602.
(34) Huang, T. W.; Zhou, C. T.; Zhang, H.; He, X. T. Effects of higher-order Kerr nonlinearity and plasma diffraction on multiple filamentation of ultrashort laser pulses in air. *Phys. Plasmas* **2013**, *20*, 072111.
(35) Tzortzakis, S.; Prade, B.; Franco, M.; Mysyrowicz, A. Time-evolution of the plasma channel at the trail of a self-guided IR femtosecond laser pulse in air. *Opt. Commun.* **2000**, *181*, 123.
(36) Rodriguez, G.; Valenzuela, A. R.; Yellampalle, B.; Schmitt, M. J.; Kim, K.-Y. In-line holographic imaging and electron density extraction of ultrafast ionized air filaments. *J. Opt. Soc. Am. B* **2008**, *25*, 1988.
(37) Feit, M. D.; Fleck, J. A., Jr. Light propagation in graded-index optical fibers. *Appl. Opt.* **1978**, *17*, 3990−3998.
(38) Lax, M.; Batteh, J. H.; Agrawal, G. P. Channeling of intense electromagnetic beams. *J. Appl. Phys.* **1981**, *52*, 109−125.

DOI: 10.1021/acsphotonics.5b00734
ACS Photonics 2016, 3, 640−646